Chemical Science

ROYAL SOCIETY OF CHEMISTRY

EDGE ARTICLE

View Article Online
View Journal | View Issue

Cite this: *Chem. Sci.*, 2020, **11**, 5213

All publication charges for this article have been paid for by the Royal Society of Chemistry

Quantification of the mixed-valence and intervalence charge transfer properties of a cofacial metal–organic framework *via* single crystal electronic absorption spectroscopy†

Patrick W. Doheny, [a] Jack K. Clegg, [b] Floriana Tuna, [c] David Collison,[c] Cameron J. Kepert *[a] and Deanna M. D'Alessandro *[a]

Gaining a fundamental understanding of charge transfer mechanisms in three-dimensional Metal–Organic Frameworks (MOFs) is crucial to the development of electroactive and conductive porous materials. These materials have potential in applications in porous conductors, electrocatalysts and energy storage devices; however the structure–property relationships pertaining to charge transfer and its quantification are relatively poorly understood. Here, the cofacial Cd(II)-based MOF [Cd(BPPTzTz)(tdc)]·2DMF (where BPPTzTz = 2,5-bis(4-(pyridin-4-yl)phenyl)thiazolo[5,4-*d*]thiazole, tdc^{2-} = 2,5-thiophene dicarboxylate) exhibits Intervalence Charge Transfer (IVCT) within its three-dimensional structure by virtue of the close, cofacial stacking of its redox-active BPPTzTz ligands. The mixed-valence and IVCT properties are characterised using a combined electrochemical, spectroelectrochemical and computational approach. Single crystal electronic absorption spectroscopy was employed to obtain the solid-state extinction coefficient, enabling the application of Marcus–Hush theory. The electronic coupling constant, H_{ab}, of 145 cm^{-1} was consistent with the localised mixed-valence properties of both this framework and analogous systems that use alternative methods to obtain the H_{ab} parameter. This work demonstrates the first report of the successful characterisation of IVCT in a MOF material using single crystal electronic absorption spectroscopy and serves as an attractive alternative to more complex methods due to its simplicity and applicability.

Received 13th March 2020
Accepted 20th April 2020

DOI: 10.1039/d0sc01521k

rsc.li/chemical-science

Introduction

The study of charge transfer in solid-state materials has received strong attention in recent years with respect to both fundamental and applied investigations. Metal–Organic Frameworks (MOFs) are porous assemblies that offer a versatile platform for the study of charge transfer in 3D materials by virtue of their porosity, tunability and long-range order.[1,2] The ability to engineer MOF materials with intrinsic charge transfer properties is attractive for many applications that harness electron transfer, such as conductivity,[3–6] electrocatalysis,[7–10] magnetism[5,11–14] and chemiresistive sensing.[15–18] Despite this, long-range charge delocalisation in 3D materials has proven difficult to achieve, often due to the intrinsically insulating nature of the organic components, the closed-shell nature of the metal ions (*i.e.* Zn(II), Cd(II), Zr(IV)) and structural instability triggered by the oxidation or reduction of the structural components.

Strategies for inducing electroactive properties in framework materials include the incorporation of redox-active metal nodes, organic ligands with electroactive functionalities (*e.g.* TTF, TCNQ) or a combination of both.[3,19] Such approaches typically harness a charge-hopping mechanism in which charge carriers (electrons or holes) 'hop' between donor and acceptor units in the extended structure, and this hopping has been extensively characterised in a number of literature reports.[20–23] Recently, it has been shown that favourable charge transfer properties leading to long-range conductivity can be engineered within MOF materials through mixed-valence interactions within the solid-state structure that give rise to Intervalence Charge Transfer (IVCT). Although only recently described and investigated in the context of MOFs,[24] IVCT and mixed valency are historically well-known phenomena, and are responsible for the characteristic colour of Prussian blue, the semiconducting

[a]*School of Chemistry, The University of Sydney, New South Wales, 2006, Australia. E-mail: deanna.dalessandro@sydney.edu.au; cameron.kepert@sydney.edu.au; Tel: +61 2 93513777*

[b]*School of Chemistry and Molecular Biosciences, The University of Queensland, St Lucia, Queensland, 4072, Australia*

[c]*Department of Chemistry and Photon Science Institute, The University of Manchester, Manchester M13 9PL, UK*

† Electronic supplementary information (ESI) available. CCDC 1988298 and 1988299. For ESI and crystallographic data in CIF or other electronic format see DOI: 10.1039/d0sc01521k

properties of which arise from IVCT between Fe(II) and Fe(III) centres.[25]

In contrast to the metal-centred IVCT in Prussian blue, organic ligand-based IVCT in MOFs was identified by Long and co-workers, who exploited the multiple reduction states of a 2,5-dihydroxybenzoquinone (dhbq) ligand in the $[(NBu_4)_2Fe(III)_2(dhbq)_3]$ framework (where NBu_4 = tetrabutylammonium).[5] Here, IVCT occurred between $dhbq^{2-/3-}$ ligands using the Fe(III)–dhbq bonds to facilitate charge transfer and achieve a conductivity of 0.16(1) S cm^{-1}. This through-bond IVCT and associated mixed valency has since been reported in a number of other MOF materials with the relatively high conductivities attributed to the low energy barrier to charge transfer associated with IVCT.[6,11,26–28]

An alternative mechanism that facilitates IVCT and has received less attention is the so-called through-space approach where the close cofacial stacking of electroactive units facilitates IVCT between mixed-valence species *via* orbital overlap. The reported examples exhibit thiazolo[5,4-*d*]thiazole (TzTz) ligands cofacially stacked in close proximity which, upon either electrochemical or chemical reduction, facilitate IVCT.[29,30] Accessing this IVCT pathway requires the use of electroactive, sterically unhindered ligands that exhibit strong π-stacking interactions to achieve cofacial overlap.

A major challenge for the elucidation of charge transfer interactions in MOFs displaying mixed valency and IVCT is the quantitative assessment of the electronic coupling (and hence, the energy barrier to charge transfer). Although mixed valency can be classified by the Robin–Day scheme,[31] and can be modelled using 2-state classical models such as Marcus–Hush theory,[32,33] the analysis is complicated by the solid-state nature of the materials. Specifically, although the key parameters such as the IVCT band energies, intensities and bandwidths are readily obtained from spectroscopic data, the derivation of an extinction coefficient to calculate the IVCT coupling parameter (H_{ab}) is not trivial. Kubelka–Munk theory can be applied to transmittance spectra obtained from a pressed pellet of a MOF within a KBr matrix, and has previously been used to obtain H_{ab} for mixed-valence MOFs.[29,30] However, this method is susceptible to a number of undesirable influences such as the smoothness of the pellet surface and hygroscopic nature of the KBr matrix, which can complicate analyses.

The present report describes the synthesis and characterisation of a Cd(II) analogue of a previously reported Zn(II) cofacial MOF incorporating the redox-active 2,5-bis(4-(pyridin-4-yl)phenyl)thiazolo[5,4-*d*]thiazole (BPPTzTz) ligand.[29] The [Cd(BPPTzTz)(tdc)]·2DMF (**CdTzTz**, where tdc^{2-} = 2,5-thiophene dicarboxylate) framework demonstrates mixed valency and associated IVCT properties upon electrochemical reduction. These IVCT properties were characterised using a combined structural, electrochemical, spectroelectrochemical and computational strategy to reveal the material as demonstrating through-space IVCT by virtue of its cofacially stacked BPPTzTz ligands. Quantification of the IVCT was achieved using Marcus–Hush theory in conjunction with a new approach to obtain the solid-state extinction coefficient in a MOF material using single crystal UV-Vis absorption spectroscopy.[34] This method was applied for the first time to quantify H_{ab}. The analogous $[Zn_2(BPPTzTz)_2(tdc)_2]_n$ (**ZnTzTz**) framework was analysed for comparison, with the resulting H_{ab} values derived from both the single crystal and Kubelka–Munk methods compared for consistency. In the latter case, this methodology involves the preparation of increasingly concentrated samples of MOF contained within KBr pressed pellets.[39] In our previous work on a selenium-based analogue of **ZnTzTz**,[30] significant uncertainties were introduced as a result of absorption of atmospheric moisture by the pellets, which in addition to the considerable degree of light scattering from the pellets, adversely affected the accuracy of the transmission measurements. The use of single crystal absorption circumvents these issues, representing an important advancement in the characterisation and quantification of mixed valency and IVCT in solid-state MOF materials. This new protocol provides a simplified and easily applicable method for quantifying charge transfer phenomena in MOFs.

Results and discussion

Synthesis and structure

The **CdTzTz** framework was obtained *via* solvothermal synthesis of the BPPTzTz ligand with 2,5-thiophene dicarboxylic acid (H_2tdc) and $Cd(NO_3)_2\cdot 4H_2O$ in DMF at 120 °C to yield yellow plate-like crystals. The structure of **CdTzTz** was solved and refined in the orthorhombic space group *Pcca* with an asymmetric unit consisting of a single Cd(II) centre coordinated by a BPPTzTz ligand and tdc^{2-} co-ligand producing a two-fold interpenetrated three-dimensional framework. The coordination sphere of the Cd(II) ion was characterised as a distorted pentagonal bipyramidal geometry consisting of five equatorial O-donors and two axial N-donors.[29,30] The structure has one-dimensional channels along the *a*- (Fig. 1a), *b*- (Fig. 1b) and *c*-axes that were occupied by DMF solvent molecules. As found in previously reported structures exhibiting this topology,[29,30] the material exhibits cofacially stacked BPPTzTz ligand dimers (Fig. 1c) due to the influence of both the tdc^{2-} coordination of the Cd(II) ions and aromatic π-stacking interactions between the adjacent BPPTzTz ligands.

The BPPTzTz ligands within each cofacial unit are separated by a distance of 3.786(6) Å (determined from the centroid-to-centroid distance defined using the atoms of the TzTz moiety). This distance is identical within the uncertainty limit to the inter-planar separation of 3.782(8) Å for **ZnTzTz** (noting that the separation was previously quoted as 3.80 Å, having been calculated as the average of the S···S distances on TzTz cores).[29] Although the TzTz moiety and one of the phenyl rings were disordered across two orientations, the backbones of the BPPTzTz ligands were found to be planar with the outer pyridyl rings offset by 19.1 and 19.7° relative to the TzTz core respectively. The solvent accessible crystal void space was calculated by PLATON[35] to be 32.7%. The TGA of **CdTzTz** (ESI, Fig. S2†) demonstrated an 18% mass loss at 213 °C, which was attributed to the loss of DMF occluded in the pore space followed by continual mass losses beyond this due to decomposition of the structure.

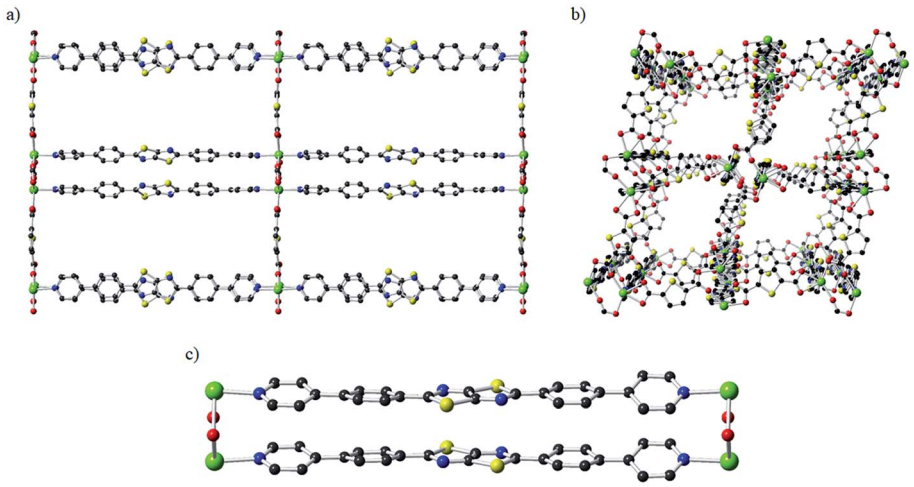

Fig. 1 Crystal structure of **CdTzTz** showing 1D channels viewed down the (a) *a*-axis and (b) *b*-axis and (c) the cofacial BPPTzTz ligand pair. Only one of the two interpenetrated networks is shown with both the disorder components and the hydrogen atoms omitted for clarity. Atom labelling: Cd = lime, S = yellow, O = red, N = blue and C = grey.

Electroactive properties

Cyclic voltammetry on **CdTzTz** in 0.1 M $[(n\text{-}C_4H_9)_4N]PF_6$/MeCN supporting electrolyte was used to characterise the electrochemical properties of the bulk material. The electrochemistry of the framework (Fig. 2) was found to be dominated by the BPPTzTz ligand with two broad cathodic process at −2.16 and −2.39 V *vs.* Fc/Fc^+. These processes were assigned to two one-electron reductions of the TzTz moiety of the BPPTzTz ligand to the radical anion and subsequent dianion state. The second process was found to be irreversible while the first was *quasi*-reversible and became reversible at faster scan rates (ESI, Fig. S3†).

Spectroelectrochemical properties

The nature of the BPPTzTz radical anion in both the discrete ligand and **CdTzTz** MOF was examined using solid-state X-band EPR spectroelectrochemistry in 0.1 M $[(n\text{-}C_4H_9)_4N]PF_6$/MeCN supporting electrolyte. The EPR spectroelectrochemical experiment on the discrete BPPTzTz ligand (Fig. 3a) revealed a 5-line signal upon reduction at −1.7 V and was characterised by an isotropic *g*-value of 2.0041, consistent with the formation of an organic radical. Numerical simulation of the signal (ESI, Fig. S4†) showed that the radical spin was coupled with two ^{14}N nuclei to yield the 5-line hyperfine splitting. Coupling constants of 5.2 MHz (0.18 mT) and 4.8 MHz (0.17 mT) were assigned to the ^{14}N nuclei of the TzTz moiety suggesting localisation of the anionic radical to the central core of the discrete ligand.

EPR spectroelectrochemistry of **CdTzTz** (Fig. 3b) revealed the *in situ* formation of an electrochemically generated radical species upon reduction. Initially EPR silent, a weak signal was observed at an applied potential of −1.8 V, which increased in intensity up to −2.0 V. The broad, isotropic signal was simulated (ESI, Fig. S5†) with a *g*-value of 2.0147 that was attributed to the formation of the BPPTzTz organic radical upon reduction. Despite hyperfine coupling of the BPPTzTz radical anion being observed in the discrete ligand, this was not observed in **CdTzTz**, presumably due to the broadness of the signal (peak-to-peak linewidth, ΔB_{p-p} = 5.2 G), which prevented the resolution of any hyperfine splitting.

The optical properties of **CdTzTz** and its radical anion state were further examined using *in situ* UV-Vis-NIR spectroelectrochemistry. The initial diffuse reflectance spectrum at 0 V (Fig. 4a) was characterised by a single band centred at 23 150 cm^{-1} (432 nm) that was assigned to the aromatic $\pi \rightarrow \pi^*$ transitions of the BPPTzTz ligand. Upon changing the applied potential from 0 to −2.2 V (Fig. 4b), this band underwent a slight blue-shift to 23 210 cm^{-1} (431 nm) with two new bands forming in the visible region at 14 930 (670 nm) and 16 640 cm^{-1} (601 nm), that were assigned to the formation of the BPPTzTz radical anion. In addition, two broad bands also appeared in the NIR region that were centred at 6930 (1443 nm) and 7550 cm^{-1} (1325 nm). A colour change of the initially bright yellow solid to dark green was also observed upon reduction. Returning the potential

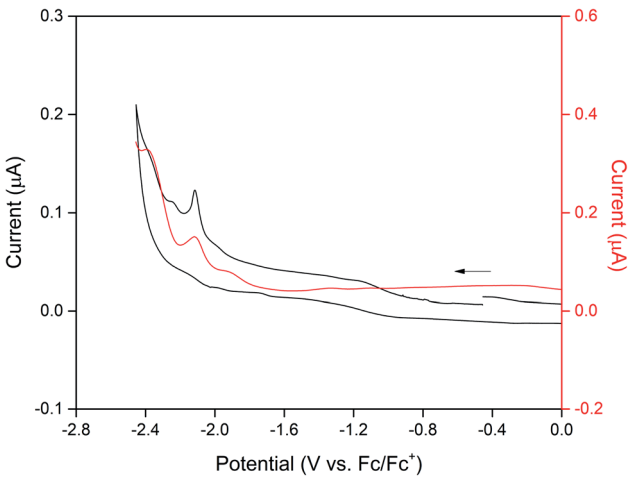

Fig. 2 Cyclic voltammetry of **CdTzTz** in 0.1 M $[(n\text{-}C_4H_9)_4N]PF_6$/MeCN supporting electrolyte at a scan rate of 25 mV s^{-1} and square wave voltammogram (red trace) where the arrow indicates the direction of the forward scan.

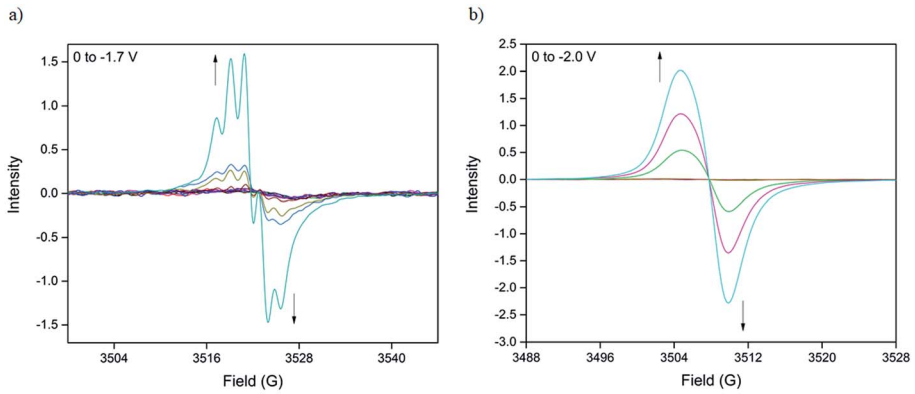

Fig. 3 (a) Solid-state EPR spectroelectrochemistry of **CdTzTz** in 0.1 M $[(n\text{-}C_4H_9)_4N]PF_6$/MeCN supporting electrolyte at potentials of 0 to −2.0 V where the arrows indicate the direction of the spectral evolution and (b) experimental *vs.* simulated spectra at −2.0 V.

to 0 V (ESI, Fig. S7†) resulted in a partial restoration of the spectrum of the neutral compound, however, weak visible and NIR bands were still evident, which may reflect the *quasi*-reversible nature of the framework reduction process.

The appearance of bands in the NIR region is characteristic of low energy IVCT interactions that arise from charge transfer between the formally neutral and radical anion BPPTzTz ligands that are in a mixed-valence state. Such IVCT properties have previously been reported in solid-state framework materials exhibiting cofacially stacked redox-active units.[29,30]

Computational modelling

Characterisation of the optical transitions observed in the UV-Vis-NIR spectroelectrochemical experiment was carried out using single point Time-Dependent Density Functional Theory (TD-DFT) calculations. The model system consisted of a cofacial dimer of BPPTzTz ligands extracted from the **CdTzTz** structure without modification except for the removal of crystallographic disorder components. TD-DFT calculations were performed using the BMK/6-311G(d) method[36] and basis set with the effects of solvation considered using a SMD[37] solvent continuum for acetonitrile. The UV-Vis-NIR spectrum was simulated for the single reduced (Fig. 5a) cofacial dimer to give good agreement between theory and experiment. Examination of the Kohn–Sham orbitals corresponding to the two calculated excited states revealed that the NIR transitions were characterised by a mixture of inter- and intra-ligand charge transfer within the cofacial unit. Such charge transfer can be assigned as through-space IVCT between a formally neutral and singly reduced BPPTzTz ligand pair within the cofacial units. From the TD-DFT analysis, the lowest energy transition was assigned to a SOMO → LUMO transition (Fig. 5b) and the second to a SOMO → LUMO+1 transition (Fig. 5c).

The calculated transitions were found to exhibit differences relative to those calculated previously for the parent Zn(II)-based material, **ZnTzTz**.[29] While the calculated NIR excited states and their corresponding orbitals showed transitions with inter- and intra-ligand character in **ZnTzTz**,[29] the two excited states calculated for **CdTzTz** both consisted of mixtures of both inter- and intra-ligand character. This may reflect the nature of the IVCT interactions in response to the structural changes induced by using the larger Cd(II) in place of Zn(II). Given the known distance-

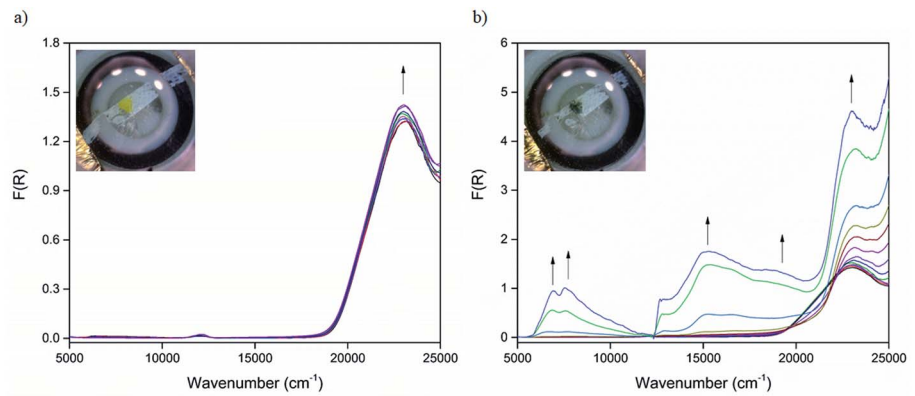

Fig. 4 Solid-state UV-Vis-NIR spectroelectrochemistry of **CdTzTz** showing potential changes from (a) 0 to −0.9 V and (b) −0.9 to −2.2 V in 0.1 M $[(n\text{-}C_4H_9)_4N]PF_6$/MeCN supporting electrolyte where the arrows indicate the direction of the spectral progression. The step at 12 500 cm^{-1} is due to a detector change. Insets: photographs of the sample acquired *in situ* during the time-course of the experiment showing a colour change from bright yellow (neutral) to dark green (mixed-valence state).

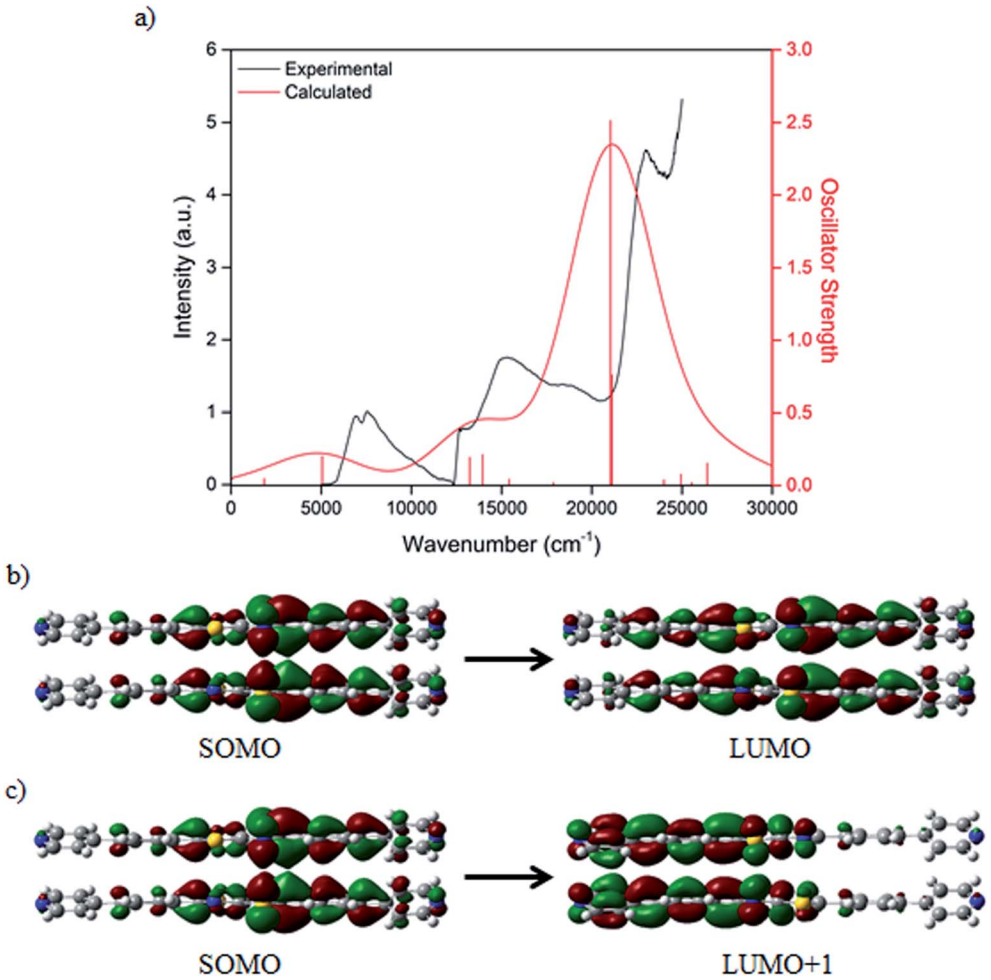

Fig. 5 (a) Experimental and calculated TD-DFT electronic absorption spectrum of the singly reduced 'model system' for the **CdTzTz** framework with predicted lineshape (black) and selected electronic transitions (red) and BMK/6-311G(d) molecular orbitals of the (b) first and (c) second calculated NIR transitions in the singly reduced cofacial BPPTzTz dimer pair.

dependence of the IVCT exhibited by these systems,[29] it is interesting to note that the inter-ligand distances in **CdTzTz** (3.786(6) Å) and **ZnTzTz** (3.782(8) Å) are identical within the uncertainty limit.

Quantification of intervalence charge transfer

The quantification of the experimentally observed mixed valency and IVCT was achieved using Marcus–Hush analysis of the NIR bands.[32,33] Deconvolution of the diffuse reflectance spectrum (ESI, Fig. S8†) from the UV-Vis-NIR spectroelectrochemical experiment obtained at an applied voltage of −2.2 V revealed that the NIR manifold was composed of four Gaussian components with the relevant spectral parameters for the first component shown in Table 1. The electronic coupling constant, H_{ab}, was evaluated using the Gaussian components obtained from deconvolution and a solid-state extinction coefficient obtained from single crystal UV-Vis absorption spectroscopy of the neutral **CdTzTz** framework (see ESI, Fig. S9a† for a description of the methodology). Single crystals of **CdTzTz** and **ZnTzTz** of dimensions 0.033 × 0.072 × 0.286 mm and 0.041 × 0.051 × 0.084 mm respectively were used to collect the absorption spectrum. For the purposes of comparison, the H_{ab} parameter for the parent **ZnTzTz** material[29] was also evaluated using same method (ESI, Fig. S9b†).

Table 1 Spectral data and charge transfer parameters derived from Marcus–Hush theory for the IVCT band (*i.e.* the lowest energy component of the NIR band manifold[a]) in the **ZnTzTz** and **CdTzTz** materials

Parameter	**ZnTzTz**[29]	**CdTzTz**
IVCT band energy,[a] ν_{max} (cm^{-1})	6576	6786
Molar extinction coefficient (M^{-1} cm^{-1})	37.3	108.8
Bandwidth-at-half-height (cm^{-1})	1465	976
Theoretical bandwidth-at-half-height (cm^{-1})	3898	3959
H_{ab} (cm^{-1})	103	145
Tunnelling matrix element T_{da} (eV)	0.00325	0.0046
Frequency factor ν_{et} (s^{-1})	1.23×10^{12}	2.43×10^{12}
Charge mobility k (s^{-1})	4.64×10^{8}	7.12×10^{8}

[a] Note that the IVCT band is defined here as the lowest energy component of the NIR band manifold, however, this component contains significant intramolecular charge transfer character in **CdTzTz**, and the H_{ab} values should thus be considered as upper limits.

For **CdTzTz**, applying the Marcus–Hush equations to these data yielded a H_{ab} value for the lowest energy component of the NIR band at $\nu_{max} = 6786\ cm^{-1}$ (1474 nm) of 145 cm^{-1}. Note that this value should be regarded as an upper limit given that the band also contains intramolecular charge transfer character. Given that the derived $2H_{ab} \ll \nu_{max}$, the IVCT transitions were assigned as arising from Robin–Day Class II mixed valency,[31] which is consistent with the assignments reported for analogous compounds using different methods to obtain solid-state extinction coefficients.[29,30] The relatively low magnitude of the electronic coupling is typical of such Class II systems where the charge transfer interactions are weak compared to mixed-valence systems that exhibit charge delocalisation such as the Creutz–Taube ion.[38] Furthermore, the H_{ab} of 103 cm^{-1} obtained for the parent **ZnTzTz** material was found to be in good agreement with the value of 123 cm^{-1} obtained using Kubelka–Munk analysis.[29,39] The charge mobilities for the mixed-valence **CdTzTz** and **ZnTzTz** systems were also found to be comparable in magnitude (4.64×10^8 *vs.* $7.12 \times 10^8\ s^{-1}$), which is consistent with the similar stacking distances between the BPPTzTz ligands in each case. The consistency between the H_{ab} values for **ZnTzTz** obtained using the Kubelka–Munk analysis and single crystal electronic absorption spectroscopy for quantifying the IVCT properties of solid-state MOF materials is encouraging. This result demonstrates the first successful application of single crystal spectroscopy absorption spectroscopy to obtain the electronic coupling parameters for a MOF material. In contrast to other reported methods that utilise transmittance measurements of pressed pellets to derive an extinction coefficient by applying Kubelka–Munk theory,[39] this simplified technique serves as an attractive alternative due to its simplicity and applicability.

Conclusions

The mixed-valence IVCT and structure–property relationships of a Cd(II)-based framework were investigated using a combined experimental and computational approach. The origin of the mixed valency was the cofacial stacking of electroactive BPPTzTz ligands within the solid-state structure, the close proximity of which enabled through-space IVCT. *In situ* UV-Vis-NIR spectroelectrochemistry of the reduced **CdTzTz** material enabled the characterisation of a mixed-valence state with NIR bands indicative of IVCT within the framework structure. Subsequent computational analysis of the NIR transitions revealed the observed IVCT as arising from the cofacial stacking motif of the BPPTzTz ligands which, upon electrochemical reduction, establish a neutral/singly reduced dimer pair.

This through-space IVCT mechanism, previously reported in analogous cofacial MOF materials,[29,30] was classified as a Robin–Day Class II system and quantified using Marcus–Hush theory. The derivation of the IVCT electronic coupling constant, H_{ab}, was achieved by extracting a solid-state extinction coefficient from the neutral MOF using single crystal electronic absorption spectroscopy. The application of this extinction coefficient to Marcus–Hush theory yielded a H_{ab} of 145 cm^{-1}, the value of which was consistent with Class II mixed valency and with the electronic coupling constants for analogous cofacial MOFs derived from alternate analytical methods.[29,30]

The determination of a solid-state extinction coefficient from single crystal absorption spectroscopy provides a new methodology for the quantification of mixed valency and IVCT in solid-state MOF materials. This simpler and more generally applicable strategy facilitates the quantitative characterisation and improved theoretical understanding of charge transfer interactions in MOF materials.

Experimental

Materials

All reagents and solvents employed were obtained from commercial sources and were used without further purification unless otherwise stated while the BPPTzTz ligand was synthesised from a previously published procedure.[29] Acetonitrile used in electrochemistry experiments was dried over CaH_2 and distilled under N_2 prior to use.

General methods

Solution-state ^1H and ^{13}C NMR spectra were recorded on a Bruker AVANCEIII 300 MHz spectrometer at 298 K. Deuterated solvents were obtained from Cambridge Stable Isotopes and were used as received with the chemical shifts (δ) referenced internally to the residual solvent resonances and quoted in ppm. PXRD data were collected with a PANanalytical X'Pert PRO diffractometer producing Cu-Kα ($\lambda = 1.5406$ Å) radiation and equipped with a solid state PIXcel detector. Mass spectrometry was performed at the Mass Spectrometry Analysis Facility at the University of Sydney on a Bruker amaZon SL mass spectrometer. Elemental microanalysis was carried out at the Chemical Analysis Facility – Element Analysis Service in the Department of Chemistry and Biomolecular Science at Macquarie University, Australia.

Framework synthesis

[Cd(BPPTzTz)(tdc)]·2DMF (CdTzTz). BPPTzTz (25.0 mg, 56.0 μmol), H_2tdc (19.2 mg, 0.11 mmol) and $Cd(NO_3)_2 \cdot 4H_2O$ (34.5 mg, 0.11 mmol) were combined in DMF (10 mL) and heated at 120 °C for 16 h. After cooling to room temperature, the crude product was washed several times with DMF before being dried *in vacuo* to give the target compound as an orange solid (37 mg, 0.04 mmol, 76% based on BPPTzTz). Elemental analysis: found C 43.8%, H 3.17%, N 7.22%, S 10.76%; calculated for $C_{32}H_{18}N_4O_4S_3Cd \cdot 2DMF \cdot 9.5H_2O$: C 43.5%, H 4.90%, N 8.02%, S 9.18%. Note: it is often difficult to obtain accurate CHNS elemental analysis data of porous framework materials due to uncertainty in their guest content at the time of measurement. The calculated formula $C_{32}H_{18}N_4O_4S_3Cd \cdot 2DMF \cdot 9.5H_2O$ thus considers that atmospheric water has entered the framework pores upon exposure to air.

Physical characterisation and instrumentation

Single crystal X-ray diffraction. Data were collected using either a Rigaku XtaLAB Synergy-S diffractometer equipped with

a Pilatus 300K detector and employing monochromated Mo-Kα radiation from a sealed X-ray tube[40] or at the MX2 beamline of the Australian Synchrotron.[41] All data were collected at 100(2) K and the structure was solved using SHELXT[42] with further structural refinements carried out using SHELXL-2018/3 (ref. 43) within the ShelXle graphical user interface.[44] Non-hydrogen atoms were refined anisotropically and hydrogen atoms placed using a riding model. Crystallographic data are given in Tables S1 and S2† and CIFs have been deposited with the CSD (CCDC 1988298 and 1988299).

Electrochemistry. Electrochemical measurements on solid materials were performed using a BASi Epsilon Electrochemical Analyser. Measurements were recorded using a three electrode set-up consisting of a glassy carbon working electrode, a platinum wire auxiliary electrode and an Ag/Ag^+ *quasi*-reference electrode in 0.1 M $[(n\text{-}C_4H_9)_4N]PF_6$/MeCN supporting electrolyte that was degassed with Ar. The sample was mounted by dipping the glassy carbon working electrode into a paste of the powdered sample in MeCN. Ferrocene was added at the completion of each experiment as an internal standard with all potentials quoted as V *vs.* Fc/Fc^+.

EPR spectroelectrochemistry. The procedure and cell set-up used were as previously reported for solid-state EPR spectroelectrochemical experiments.[29,45,46] Briefly, a three electrode set-up consisting of a platinum wire working and auxiliary electrode each with a platinum mesh attached to the ends and a silver wire *quasi*-reference electrode. The wires were coated with Teflon to prevent short-circuiting with the bottom 1 cm of each wire stripped, with the exception of the auxiliary electrode wire that was completely bare. The sample was immobilised on a platinum mesh connected to the end of the platinum wire working electrode and inserted into a cell consisting of a flame-sealed pipette with the exposed wires well separated. The potential was controlled using an μAutolab II potentiostat with 0.1 M $[(n\text{-}C_4H_9)_4N]PF_6$/MeCN used for all measurements. Continuous wave X-band EPR spectra were recorded using a Bruker EMX Micro spectrometer equipped with a 1.0 T electromagnet with the microwave power and attenuation tuned to prevent signal saturation. The EPR signals obtained were referenced to strong pitch to obtain the *g*-value and spectral simulations were carried out using the Easyspin simulation package.[47]

UV-Vis-NIR spectroelectrochemistry. UV-Vis-NIR spectroelectrochemistry of bulk materials was carried out using a CARY5000 spectrophotometer equipped with a Harrick Omni-Diff probe attachment. The Teflon® spectroelectrochemical cell consisted of a platinum *quasi*-reference electrode, a silver wire auxiliary electrode and an indium–tin-oxide (ITO) coated glass slide working electrode as reported previously.[48] The sample was immobilised on the conductive side of the ITO slide using Teflon® tape and the applied potential controlled using an eDAQ e-corder 410 potentiostat. 0.1 M $[(n\text{-}C_4H_9)_4N]PF_6$/MeCN supporting electrolyte was used for all measurements with all spectral data reported as the Kubelka–Munk transform, where $F(R) = (1 - R)^2/2R$ (where R is the diffuse reflectance of the sample relative to the Teflon baseline).

Single crystal UV-Vis spectroscopy. Polarised single crystal UV-Vis spectroscopy was performed using a customised spectrophotometer described in a previous publication by Krausz.[34] The apparatus was composed of optics obtained from a CARY14 spectrophotometer equipped with a 24 V/150 W quartz halogen lamp and a Spec 1704, 1 m, high-resolution Czerny–Turner monochromator with 500, 1000 and 1600 nm gratings and a fitted high-speed stepper motor. A single crystal was mounted over a 1 mm aperture and data were collected over a 300–650 nm energy range in both horizontal and vertical polarisation modes. A baseline correction was applied to the data by measuring the absorbance spectra of the empty aperture, which was then manually subtracted from the absorption spectra of the crystal.

Computational details. Single point density functional theory (DFT) and time-dependent density functional theory (TD-DFT) calculations were carried out using the Gaussian 16 software suite.[49] The UV-Vis-NIR spectra of the **CdTzTz** framework was calculated using the BMK/6-311G(d) method[36] and basis set with solvation effects considered using the SMD continuum model[37] with parameters for acetonitrile. The computational model consisted of a cofacial pair of BPPTzTz ligands extracted directly from the **CdTzTz** crystal structure without modification, but with the removal of disordered components. The orbital transitions responsible for the calculated NIR excited states were assigned using the dominant contribution to each excited state and visual inspection of the associated molecular orbitals.

Conflicts of interest

There are no conflicts to declare.

Acknowledgements

We gratefully acknowledge support from the Australian Research Council (ARC) for research funding. This research was undertaken with the assistance of resources and services from the MX2 beamline at the Australian Synchrotron, part of ANSTO, and made use of the Australian Cancer Research Foundation (ACRF) detector and the National Computational Infrastructure (NCI), which are supported by the Australian Government. This research was also supported with the use of the X-ray powder diffraction services of the Sydney Analytical Core Facility at the University of Sydney. We thank EPSRC (UK) for funding the National Research Facility (NRF) for EPR Spectroscopy at Manchester. The authors would like to thank Harrison Moore (USyd) and Emeritus Professor Elmars Krausz (Australian National University) for assistance and helpful discussions regarding the single crystal UV-Vis absorption spectroscopy analysis.

References

1 B. F. Hoskins and R. Robson, *J. Am. Chem. Soc.*, 1990, **112**, 1546.
2 H. Li, M. Eddaoudi, M. O'Keeffe and O. M. Yaghi, *Nature*, 1999, **402**, 276.

3 D. M. D'Alessandro, *Chem. Commun.*, 2016, **52**, 8957.
4 L. Sun, C. H. Hendon and M. Dincă, *Dalton Trans.*, 2018, **47**, 11739.
5 L. E. Darago, M. L. Aubrey, C. J. Yu, M. I. Gonzalez and J. R. Long, *J. Am. Chem. Soc.*, 2015, **137**, 15703.
6 J. G. Park, M. L. Aubrey, J. Oktawiec, K. Chakarawet, L. E. Darago, F. Grandjean, G. J. Long and J. R. Long, *J. Am. Chem. Soc.*, 2018, **140**, 8526.
7 B. A. Johnson, A. Bhunia, H. Fei, S. M. Cohen and S. Ott, *J. Am. Chem. Soc.*, 2018, **140**, 2985.
8 F.-L. Li, Q. Shao, X. Huang and J.-P. Lang, *Angew. Chem., Int. Ed.*, 2018, **57**, 1888.
9 P.-Q. Liao, J.-Q. Shen and J.-P. Zhang, *Coord. Chem. Rev.*, 2018, **373**, 22.
10 A. J. Clough, J. W. Yoo, M. H. Mecklenburg and S. C. Marinescu, *J. Am. Chem. Soc.*, 2015, **137**, 118.
11 J. A. DeGayner, I.-R. Jeon, L. Sun, M. Dincă and T. D. Harris, *J. Am. Chem. Soc.*, 2017, **139**, 4175.
12 L. Liu, J. A. DeGayner, L. Sun, D. Z. Zee and T. D. Harris, *Chem. Sci.*, 2019, **10**, 4652.
13 H. Miyasaka, N. Motokawa, S. Matsunaga, M. Yamashita, K. Sugimoto, T. Mori, N. Toyota and K. R. Dunbar, *J. Am. Chem. Soc.*, 2010, **132**, 1532.
14 G. Mínguez Espallargas and E. Coronado, *Chem. Soc. Rev.*, 2018, **47**, 533.
15 M. G. Campbell, S. F. Liu, T. M. Swager and M. Dincă, *J. Am. Chem. Soc.*, 2015, **137**, 13780.
16 M. E. Dmello, N. G. Sundaram, A. Singh, A. K. Singh and S. B. Kalidindi, *Chem. Commun.*, 2019, **55**, 349.
17 W.-T. Koo, J.-S. Jang and I.-D. Kim, *Chem*, 2019, **5**, 1938.
18 S. Wang, J. Liu, H. Zhao, Z. Guo, H. Xing and Y. Gao, *Inorg. Chem.*, 2018, **57**, 541.
19 R. Murase, B. Ding, Q. Gu and D. M. D'Alessandro, *Philos. Trans. R. Soc., A*, 2019, **377**, 20180226.
20 C. F. Leong, B. Chan, T. B. Faust and D. M. D'Alessandro, *Chem. Sci.*, 2014, **5**, 4724.
21 T. C. Narayan, T. Miyakai, S. Seki and M. Dincă, *J. Am. Chem. Soc.*, 2012, **134**, 12932.
22 S. S. Park, E. R. Hontz, L. Sun, C. H. Hendon, A. Walsh, T. Van Voorhis and M. Dincă, *J. Am. Chem. Soc.*, 2015, **137**, 1774.
23 S. Lin, P. M. Usov and A. J. Morris, *Chem. Commun.*, 2018, **54**, 6965.
24 R. Murase, C. F. Leong and D. M. D'Alessandro, *Inorg. Chem.*, 2017, **56**, 14373.
25 D. R. Rosseinsky, J. S. Tonge, J. Berthelot and J. F. Cassidy, *J. Chem. Soc., Faraday Trans. 1*, 1987, **83**, 231.
26 C. J. Kingsbury, B. F. Abrahams, D. M. D'Alessandro, T. A. Hudson, R. Murase, R. Robson and K. F. White, *Cryst. Growth Des.*, 2017, **17**, 1465.
27 R. Murase, B. F. Abrahams, D. M. D'Alessandro, C. G. Davies, T. A. Hudson, G. N. L. Jameson, B. Moubaraki, K. S. Murray, R. Robson and A. L. Sutton, *Inorg. Chem.*, 2017, **56**, 9025.
28 M. L. Aubrey, B. M. Wiers, S. C. Andrews, T. Sakurai, S. E. Reyes-Lillo, S. M. Hamed, C.-J. Yu, L. E. Darago, J. A. Mason, J.-O. Baeg, F. Grandjean, G. J. Long, S. Seki, J. B. Neaton, P. Yang and J. R. Long, *Nat. Mater.*, 2018, **17**, 625.
29 C. Hua, P. W. Doheny, B. Ding, B. Chan, M. Yu, C. J. Kepert and D. M. D'Alessandro, *J. Am. Chem. Soc.*, 2018, **140**, 6622.
30 B. Ding, C. Hua, C. J. Kepert and D. M. D'Alessandro, *Chem. Sci.*, 2019, **10**, 1392.
31 M. B. Robin and P. Day, in *Adv. Inorg. Chem. Radiochem.*, ed. H. J. Emeléus and A. G. Sharpe, Academic Press, 1968, vol. 10, p. 247.
32 G. C. Allen and N. S. Hush, *Prog. Inorg. Chem.*, 1967, **8**, 357.
33 N. S. Hush, *Prog. Inorg. Chem.*, 1967, **8**, 391.
34 E. Krausz, *Aust. J. Chem.*, 1993, **46**, 1041.
35 A. Spek, *Acta Crystallogr., Sect. D: Biol. Crystallogr.*, 2009, **65**, 148.
36 A. D. Boese and J. M. L. Martin, *J. Chem. Phys.*, 2004, **121**, 3405.
37 A. V. Marenich, C. J. Cramer and D. G. Truhlar, *J. Phys. Chem. B*, 2009, **113**, 6378.
38 C. Creutz and H. Taube, *J. Am. Chem. Soc.*, 1973, **95**, 1086.
39 P. Kubelka, *J. Opt. Soc. Am.*, 1948, **38**, 448.
40 Rigaku Oxford Diffraction, *CrysAlisPro*, Yarnton, Oxfordshire, England, 2014.
41 D. Aragao, J. Aishima, H. Cherukuvada, R. Clarken, M. Clift, N. P. Cowieson, D. J. Ericsson, C. L. Gee, S. Macedo, N. Mudie, S. Panjikar, J. R. Price, A. Riboldi-Tunnicliffe, R. Rostan, R. Williamson and T. T. Caradoc-Davies, *J. Synchrotron Radiat.*, 2018, **25**, 885.
42 G. Sheldrick, *Acta Crystallogr., Sect. A: Found. Crystallogr.*, 2015, **71**, 3.
43 G. Sheldrick, *Acta Crystallogr., Sect. C: Struct. Chem.*, 2015, **71**, 3.
44 C. B. Hubschle, G. M. Sheldrick and B. Dittrich, *J. Appl. Crystallogr.*, 2011, **44**, 1281.
45 P. R. Murray, D. Collison, S. Daff, N. Austin, R. Edge, B. W. Flynn, L. Jack, F. Leroux, E. J. L. McInnes, A. F. Murray, D. Sells, T. Stevenson, J. Wolowska and L. J. Yellowlees, *J. Magn. Reson.*, 2011, **213**, 206.
46 C. Hua, A. Baldansuren, F. Tuna, D. Collison and D. M. D'Alessandro, *Inorg. Chem.*, 2016, **55**, 7270.
47 S. Stoll and A. Schweiger, *J. Magn. Reson.*, 2006, **178**, 42.
48 P. M. Usov, C. Fabian and D. M. D'Alessandro, *Chem. Commun.*, 2012, **48**, 3945.
49 M. J. Frisch, G. W. Trucks, H. B. Schlegel, G. E. Scuseria, M. A. Robb, J. R. Cheeseman, G. Scalmani, V. Barone, G. A. Petersson, H. Nakatsuji, X. Li, M. Caricato, A. V. Marenich, J. Bloino, B. G. Janesko, R. Gomperts, B. Mennucci, H. P. Hratchian, J. V. Ortiz, A. F. Izmaylov, J. L. Sonnenberg, D. Williams-Young, F. Ding, F. Lipparini, F. Egidi, J. Goings, B. Peng, A. Petrone, T. Henderson, D. Ranasinghe, V. G. Zakrzewski, J. Gao, N. Rega, G. Zheng, W. Liang, M. Hada, M. Ehara, K. Toyota, R. Fukuda, J. Hasegawa, M. Ishida, T. Nakajima, Y. Honda, O. Kitao, H. Nakai, T. Vreven, K. Throssell, J. A. Montgomery Jr, J. E. Peralta, F. Ogliaro, M. J. Bearpark, J. J. Heyd, E. N. Brothers, K. N. Kudin, V. N. Staroverov, T. A. Keith, R. Kobayashi, J. Normand, K. Raghavachari, A. P. Rendell, J. C. Burant, S. S. Iyengar, J. Tomasi, M. Cossi, J. M. Millam, M. Klene, C. Adamo, R. Cammi, J. W. Ochterski, R. L. Martin, K. Morokuma, O. Farkas, J. B. Foresman and D. J. Fox, *Gaussian 16 Revision A. 03*, Gaussian, Inc., Wallingford, CT, 2016.

